Iron complexes as electrocatalysts for the water oxidation reaction

Kottrup, K.G.

Chapter 5

Interactions between metal complexes and the electrode surface – the influence of dissolved metal complexes on the surface of gold and graphitic carbon electrodes

In this chapter, the influence of interactions between dissolved metal complexes and the surface of working electrodes made from gold and pyrolytic graphite (PG) is investigated with respect to the consequences for the electrode material. For a PG electrode, the presence of iron complexes in solution appears to facilitate the formation of CO_2 from the electrode material already at lower potentials than in blank experiments in the absence of metal complexes.

*For a gold electrode, performing cyclic voltammetry in the presence of either $[(MeOH)Fe(Hbbpya)–\mu\text{-}O–(Hbbpya)Fe(MeOH)](OTf)_4$ (**1**) (with Hbbpya = N,N-bis(2,2'-bipyrid-6-yl)amine) or $[Ru(tpy)(bpy)(H_2O)](OTf)_2$ (**2**) (with bpy = bipyridine and tpy = terpyridine) results in clear changes to the voltammogram of the gold background. These changes were found to be reversible over several scans in a subsequent cyclic voltammetry experiment with a blank electrolyte solution. The nature of these changes is not yet understood and the mechanism of the processes behind them requires further investigation.*

For both electrode materials, the effects of the presence of dissolved metal complexes are potentially highly significant, in particular for attempts at benchmarking catalysts. Therefore the interactions between the electrode surface and complexes in solution should be considered carefully in electrocatalytic applications.

Part of the results presented in this chapter have been submitted for publication: K.G. Kottrup, S. D'Agostini, P.H. van Langevelde, M.A. Siegler and D.G.H. Hetterscheid, *ACS Catal.* accepted for publication.
Other results presented in this chapter are to be submitted for publication: *manuscript in preparation*.

5.1 Introduction

Choosing the right electrode material can be a crucial aspect of setting up an electrochemical experiment. In the context of electrocatalytic water oxidation, electrodes made from carbon-based materials such as pyrolytic graphite (PG) and glassy carbon (GC) are particularly attractive because they feature a flat background across a wide potential window.[1] However, the downside of working with carbon-based materials is their propensity for CO_2 formation at higher potentials.[2] Since CO_2 formation is a useful indicator for catalyst decomposition in the case of metal complexes bearing organic ligands,[3-4] CO_2 formation from the electrode material can obscure such processes.

Another commonly used electrode material besides carbon is gold. Gold does not produce CO_2 and therefore allows to track CO_2 formation from ligand decomposition. However, gold does undergo gold oxide formation and reduction reactions which result in a considerably more complex background voltammogram compared to PG and GC. In particular polycrystalline gold electrodes show a multitude of redox events in cyclic voltammetry (CV) experiments due to the presence of several different structural features on the electrode surface. Furthermore, gold itself catalyzes the water oxidation reaction with an onset at about 2.0 V vs. a reversible hydrogen electrode (RHE).[5-6]

Other non-metallic electrode materials such as indium tin oxide (ITO), fluorine-doped tin oxide (FTO) or boron-doped diamond (BDD) are also inert over wide potential ranges.[1] However, due to their nature as semi-conductors, they exhibit a low density of states at the Fermi level which can influence electron-transfer kinetics between the electrode and the catalyst. As a result, ITO and BDD electrodes proved to be unsuitable for studying the water oxidation catalysts discussed in this thesis (cf. Fig. B.7, Appendix B and Fig. C.4, Appendix C).

The results discussed in chapter 3 and 4 show that interactions between the catalyst and the surface of a particular electrode material can significantly influence the electrochemical behaviour of the catalyst. On the other hand, the interactions between the catalyst and the electrode may also have consequences for the surface of the electrode in return. Evidence for this is also briefly discussed in chapters 3 and 4 of this thesis. The results presented in chapter 3 suggest that most of the considerable CO_2 formation that is observed throughout all OLEMS experiments with PG working electrodes, that are described in this thesis, originates from decomposition of the electrode material. The results presented in chapter 4 show an increase in the peak current at 2.0 V vs. RHE between

subsequent scans during CV experiments of α-[Fe(bpmcn)($OTf)_2$] (with bpmcn = *N*,*N*'-dimethyl-*N*,*N*'-bis(2-pyridylmethyl)-cyclohexane-1,2-diamine) in combination with a gold working electrode. This increase in current was found to be most likely due to changes of the structure of the electrode surface. Other possible explanations such as modifications of the complex in solution or deposition of solids on the electrode surface could be ruled out through control experiments. However, the nature of the changes at the gold surface remains unclear.

To the best of our knowledge, the influence of the presence of metal complexes in solution on the surface of the working electrode has so far been largely overlooked in literature on electrocatalytic water oxidation despite the potentially important implications for the field. Therefore, in this chapter, we explore the effects of the presence of metal complexes in solution on the two electrode materials gold and PG. For the case of a PG working electrode we compare the onset of CO_2 formation in OLEMS experiments, both in the absence and presence of metal complexes in solution. For the case of a gold working electrode we compare voltammograms of the gold background before and after performing cyclic voltammetry in the presence of metal complexes in solution.

5.2 Results and Discussion

5.2.1 Electrochemistry of carbon

Before investigating the behaviour of any electrode material in the presence of metal complexes, it is important to first establish the behaviour of the electrode material by itself, in the absence of any complex in solution.

A review about electrode materials for studying electrocatalysts, published in 2014, described carbon-based materials such as GC and highly ordered pyrolytic graphite (HOPG) as being inert across a large potential range.[1] In acidic and neutral electrolyte solutions, the respective usable anodic potential range was reportedly limited by the onset of oxygen evolution around 1.8 V vs. RHE in 0.1 M H_2SO_4 and around 2.0 V vs. RHE in 0.1 M NaOAc.

In contrast to that, we find that no oxygen evolution occurs at a PG working electrode in the absence of any additional catalyst in both 0.1 M $HClO_4$ (Fig. 5.1) and 0.1 M Na_2SO_4 (Fig. 5.2) electrolyte solution even at potentials well above 2.0 V. Instead, only CO_2 formation can be seen in on-line electrochemical mass spectrometry (OLEMS) experiments. Figures 5.1 and 5.2 show the corresponding mass traces of CO_2 and O_2 recorded during chronoamperometry experiments with

a PG working electrode at 1.9, 2.0 and 2.2 V in a 0.1 M $HClO_4$ electrolyte solution and a 0.1 M Na_2SO_4 electrolyte solution respectively. Based on the recorded current and the ion current in the *m/z* = 44 trace, the rate of CO_2 formation appears to be substantially higher in acidic solution compared to neutral unbuffered electrolyte solutions. This finding is in line with the work of Schlögl and co-workers who reported that GC electrodes are oxidized faster in acidic environments than in neutral environments.[7]

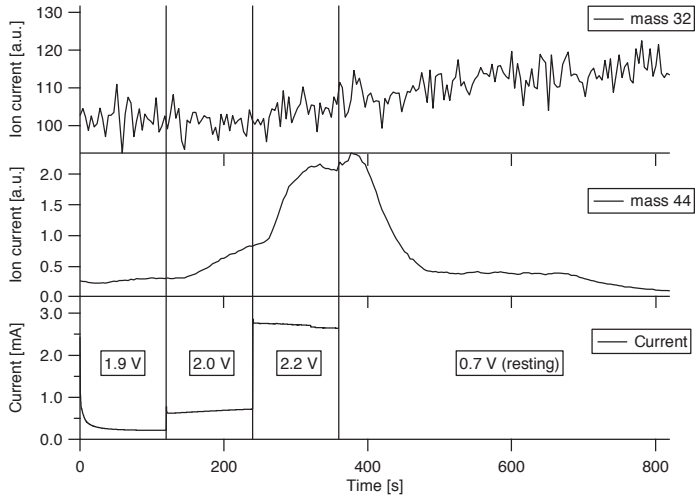

Figure 5.1: Results of an OLEMS measurement of a PG working electrode during chronoamperometry in a 0.1 M $HClO_4$ solution. Shown are the current (bottom), the *m/z* trace for CO_2 (middle) and *m/z* trace for O_2 (top) while applying different potentials for 120 seconds each. The potentials that were applied are: 1.9 V vs. RHE (0-120 s), 2.0 V vs. RHE (120-240 s) and 2.2 V vs. RHE (240-360 s). After 360 s the potential was switched to a resting potential of 0.7 V vs. RHE. The vertical lines indicate the points in time when the potential was switched.

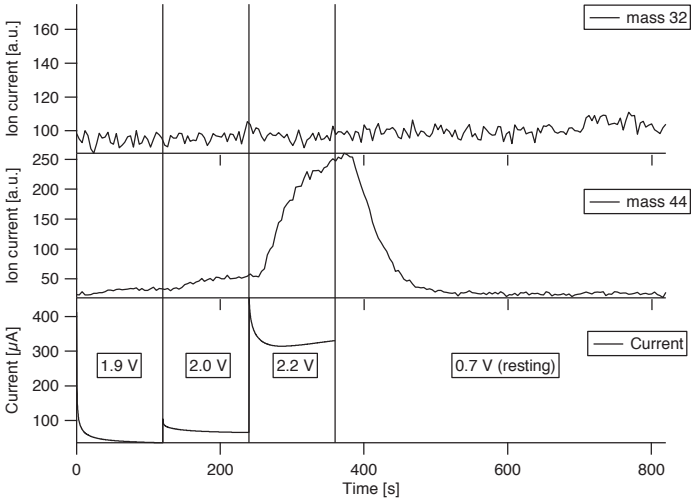

Figure 5.2: Results of an OLEMS measurement of a PG working electrode during chronoamperometry in a 0.1 M Na_2SO_4 solution. Shown are the current (bottom), the *m/z* trace for CO_2 (middle) and *m/z* trace for O_2 (top) while applying different potentials for 120 seconds each. The potentials that were applied are: 1.9 V vs. RHE (0-120 s), 2.0 V vs. RHE (120-240 s) and 2.2 V vs. RHE (240-360 s). After 360 s the potential was switched to a resting potential of 0.7 V vs. RHE. The vertical lines indicate the points in time when the potential was switched.

To determine the onset of CO_2 formation, cyclic voltammetry was performed in combination with OLEMS. Figure 5.3a shows the result of an OLEMS experiment while cycling the potential between 1.3 and 2.0 V at 1 mV/s in a blank 0.1 M Na_2SO_4 electrolyte solution. From the corresponding CO_2 mass trace an onset of CO_2 formation at about 1.9 V can be determined. In comparison to that, an earlier onset of CO_2 formation is observed when a metal complex is present in the electrolyte solution (Fig. 5.3b). In the presence of 1 mM $Fe(OTf)_2$ the OLEMS shows an onset for CO_2 formation at about 1.6 V. Similarly, all OLEMS experiments performed in combination with a PG working electrode in the presence of a metal complex, that are discussed throughout this thesis, show an onset of CO_2 evolution at potentials significantly below 1.9 V. In chapter 2, all three cyclam-based complexes showed CO_2 formation during OLEMS experiments in both unbuffered and phosphate-buffered electrolyte media (Fig. 2.6, 2.11, 2.12, chapter 2) with onset potentials of CO_2 formation as low as 1.2 V for [Fe(cyclamacetate)Cl] and 1.4 V for *cis*-[Fe(cyclam)Cl]Cl_2 (Fig. 2.6, chapter 2).

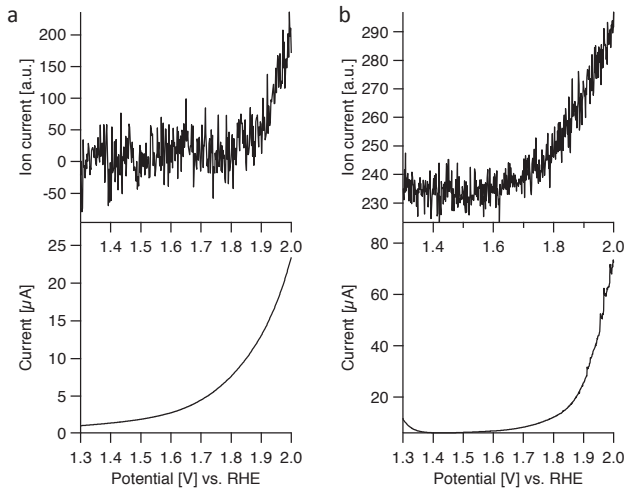

Figure 5.3: (a) Results of an OLEMS measurement with a PG working electrode during cyclic voltammetry in a blank 0.1 M $NaClO_4$ solution. Shown are the mass trace of *m/z* = 44 (top) and the current (bottom). (b) Results of an OLEMS measurement with a PG working electrode during cyclic voltammetry in a 0.1 M $NaClO_4$ solution in the presence of 1 mM $Fe(OTf)_2$. Shown are the mass trace of *m/z* = 44 (top) and the current (bottom). For the sake of clarity, only the forward scan of each measurement is depicted.

The Fe(Hbbpya) complex (Hbbpya = *N*,*N*-bis(2,2'-bipyrid-6-yl)amine), which is described in chapter 3, showed negligible CO_2 formation with a gold working electrode (Fig. 3.4, chapter 3) but substantial CO_2 formation starting at 1.6 V in combination with a PG working electrode (Fig. 3.6, chapter 3). Similarly, the Fe(bpmcn) complexes (bpmcn = *N*,*N*'-dimethyl-*N*,*N*'-bis(2-pyridylmethyl)-cyclohexane-1,2-diamine) discussed in chapter 4 also showed CO_2 formation starting at 1.5 V in combination with a PG working electrode (Fig 4.13, chapter 4) while little to no CO_2 formation was observed in combination with a gold working electrode (Fig. 4.14-4.16, chapter 4).

For most metal complexes it is difficult to pinpoint the source of the CO_2 as it might originate from decomposition of the ligand, decomposition of the electrode or both. However, in the case of $Fe(OTf)_2$ any CO_2 that is being observed in OLEMS measurements (Fig. 5.3b) must almost certainly originate from the electrode material as the only other source of carbon, which is present in the system, is the redox inert triflate ion. This demonstrates that high-valent metal oxo-species have the ability to catalyze the oxidation of carbon electrodes. As a result the performance of a water oxidation catalyst in combination with a carbon-based working electrode can be impacted negatively since part of the available catalyst does not complete the catalytic cycle towards oxygen evolution. Instead, part of

the catalyst undergoes side reactions, resulting in a lower faradaic efficiency and lower turnover frequency.

For any complex that is capable of catalyzing the water oxidation reaction, the capability to oxidize other substrates as well is certainly not unexpected as water is one of the most difficult to oxidize substrates. Therefore it seems plausible that the oxidation of substrates such as the carbon electrode itself can occur already at potentials below the onset of water oxidation. Accordingly, for all iron complexes discussed in this thesis, the onset of oxygen evolution was found to lie several hundred millivolts above the onset of CO_2 formation when using a PG working electrode. The only exception is the Fe(Hbbpya) complex described in chapter 3 for which the onsets of O_2 evolution and CO_2 formation coincide around 1.6 V in experiments with a PG working electrode. As a result, routine methods to determine catalyst kinetics such as the foot-of-the-wave (FOTW) analysis cannot always be applied without reservations.

The FOTW method is used to determine a catalyst's maximum turnover frequency by extrapolating from measurements performed near the onset of the catalytic wave.[8] Figure 5.4 shows a schematic representation of an ideal sigmoidal shaped catalytic current wave.[9] The area highlighted in green in figure 5.4 shows the current region in which the current plateaus because the maximum turnover frequency of the catalyst is reached. In this region, the turnover frequency is no longer limited by electron-transfer rates but solely by the kinetics of the rate-limiting step of the catalytic cycle. Therefore, increasing the potential further does not result in higher currents.

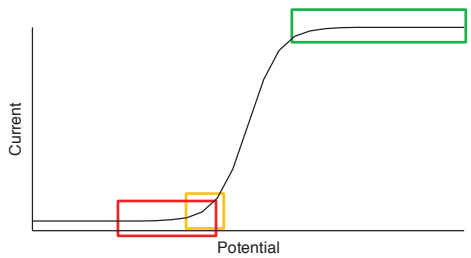

Figure 5.4: Schematic representation of an ideal sigmoidal catalytic current wave on which three different regions are highlighted: region in which current from CO_2 formation may dominate over current from water oxidation (red); region in which foot-of-the-wave analysis is performed (yellow); region in which the reaction rate is no longer limited by electron-transfer rates but by the kinetics of the catalytic reaction (green).

The resulting sigmoidal shape shown in figure 5.4 represents an ideal case in which no other factors limit the turnover frequency of the catalyst. In real electrocatalytical studies, unwanted side-effects such as substrate consumption, catalyst decomposition or product inhibition can become rate limiting and obscure the intrinsic properties of the catalyst.[9]

By using the FOTW method one seeks to calculate the theoretical maximum turnover frequency at the plateau of the sigmoidal current wave (Fig. 5.4 area highlighted in green) while avoiding the aforementioned side-effects present in real systems by focusing on the area around the onset of the catalytic wave where those effects are still negligible (Fig. 5.4, area highlighted in yellow). The results of the OLEMS experiments presented in this thesis show, however, that one also needs to rule out CO_2 formation from the electrode as a side reaction when one is working with carbon-based electrodes as CO_2 formation can contribute significantly to the current near the onset of water oxidation (Fig. 5.4, area highlighted in red).

5.2.2 Electrochemistry of gold

5.2.2a Introduction

In contrast to carbon-based electrodes, working electrodes made from gold are capable of catalyzing the water oxidation reaction even in the absence of an additional catalyst. The onset for water oxidation by a gold electrode without any additional catalyst was determined to lie at about 2 V vs. RHE under both acidic and neutral electrolyte conditions.[5-6] This limits the use of gold as an electrode material for studying water oxidation catalysts to potentials below 2 V. Aside from being able to catalyze water oxidation, gold electrodes also show a complex pattern of background redox processes associated with the formation and reduction of gold oxide[10-12] which can complicate voltammetry measurements of complexes in solution.

While structural changes at the surface of gold electrodes induced by external factors have been studied in material sciences, to the best of our knowledge, no literature currently discusses the possible consequences for electrocatalysis. Therefore, in this chapter, we discuss the effects of dissolved metal complexes on the surface of a gold working electrode and the possible implications in the context of electrocatalytic water oxidation. The effects are investigated using cyclic voltammetry measurements and comparing the observed redox features of

the background voltammogram of a gold working electrode before and after cyclic voltammetry experiments in the presence of dissolved metal complexes.

5.2.2b Blank experiments in acidic and neutral unbuffered electrolyte media

In order to assess the influences of dissolved metal complexes on the surface of a gold working electrode, it is necessary to first determine the baseline background voltammogram of a clean gold working electrode in blank electrolyte solutions in the absence of any metal complex. Background voltammograms of a gold electrode were therefore recorded in both acidic and neutral unbuffered electrolyte solutions.

At pH 1 (0.1 M $HClO_4$) and in the absence of any metal complex, a gold electrode shows several redox events in a cyclic voltammetry experiment which are related to the formation and the reduction of gold oxide (Fig. 5.5a). This observed profile is in agreement with literature.[10-12] The current profile of the forward scan of the voltammogram consists of an onset of oxidative current at about 1.3 V with a relatively sharp peak that has been attributed to the formation of hydroxyl-species on the surface of the electrode, followed by a broader peak which completes the oxidation of the electrode surface from gold to gold oxide.[10-11] In the backward scan, the reduction of gold oxide takes the shape of a sharp peak at about 1.1 V followed by a shoulder at 1.0 V. The sharp peak has been attributed to the reduction of metal oxo-species at the electrode surface while the shoulder represents the reduction of a sublattice of hydroxyl-species in between adsorbed anions.[10-11] The presence of several peaks for both gold oxide formation and gold oxide reduction is also observed for single crystal electrodes.[13] As such, it is not a feature associated with different faces on the electrode surface but rather an inherent feature of gold as a substrate.[10-11]

While there is a wealth of information about the behaviour of gold electrodes in acidic and alkaline electrolyte solutions,[13-21] comparatively little information is available about the behaviour of gold electrodes in neutral unbuffered electrolyte solutions.[12, 22-23]

CV experiments with a gold working electrode in a neutral unbuffered electrolyte solution of 0.1 M $NaClO_4$ reveal a different shape of the current profile (Fig. 5.5b). While the formation of gold oxide is again represented by a sharp peak followed by a broader peak, the reduction of gold oxide now consists of two strictly separate peaks about 500 mV apart at 1.2 and 0.7 V respectively. This shape is once again in agreement with previous reports.[12] The separation between the

two gold oxide reduction peaks has previously been attributed to local pH changes in an unbuffered solution.[13, 18]

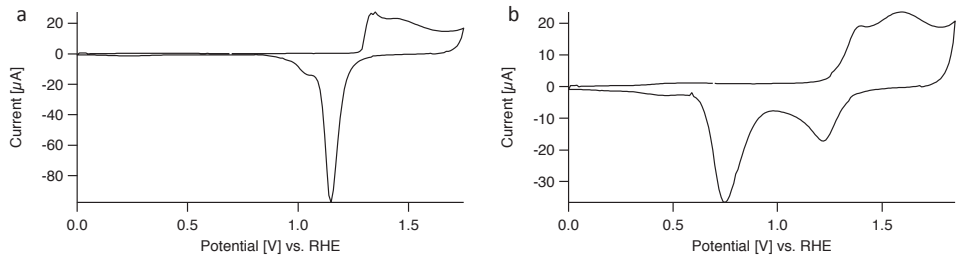

Figure 5.5: (a) Results of a CV measurement with a gold working electrode in a 0.1 M $HClO_4$ electrolyte solution, recorded between 0.0 and 1.75 V vs. RHE at 100 mV/s, starting at 0.7 V vs. RHE (b) Results of a CV measurement with a gold working electrode in a 0.1 M $NaClO_4$ electrolyte solution, recorded between 0.0 and 1.85 V vs. RHE at 100 mV/s, starting at 0.7 V vs. RHE.

5.2.2c Metal complex induced changes to the surface of a gold working electrode

In chapter 3 of this thesis, CV experiments are described with a gold working electrode in combination with 0.5 mM [(MeOH)Fe(Hbbpya)–µ-O–(Hbbpya)Fe(MeOH)](OTf)$_4$ (**1**) (with Hbbpya = *N*,*N*-bis(2,2'-bipyrid-6-yl)amine) present in the electrolyte solution. In the corresponding voltammograms, recorded in the presence of complex **1**, the current in the potential region between 1.3 and 1.9 V, which corresponds to the formation of gold oxide, follows a different profile compared to the blank experiment (compare Fig. 5.5b and Fig. 3.2d, chapter 3). In the presence of complex **1**, two broad oxidation waves are observed in the region between 1.3 and 1.9 V. In the backward scan only a single reduction peak at 1.2 V is visible. The results discussed in chapter 3 already demonstrate that this difference in oxidative current in the 1.3 to 1.9 V potential region between the presence and the absence of complex **1** is indeed related to gold oxide formation processes and not redox reactions of complex **1** itself (cf. Fig. 3.4, chapter 3).

This difference between the presence and absence of complex **1** in solution indicates that complex **1** interacts with the gold electrode in a way that influences the mechanism of gold oxide formation and gold oxide reduction. Therefore, in this chapter, the influence of metal complexes, that are present in solution, on the processes at the electrode surface is discussed. This is done by comparing the background voltammograms of a gold electrode, recorded in blank Na_2SO_4 electrolyte solutions, before and after CV experiments in the presence of complex **1**. Additionally, identical CV experiments were also performed in the presence of

0.5 mM [Ru(tpy)(bpy)(H_2O)]($OTf)_2$ (**2**) (with bpy = bipyridine and tpy = terpyridine) instead of complex **1**, to determine whether the observed effects are unique for complex **1** or whether other complexes exhibit a similar influence on the gold electrode. Since both complexes dissolve poorly in perchlorate containing electrolyte solutions, Na_2SO_4 was chosen instead as the appropriate electrolyte for all experiments with either complex.

In CV experiments with a gold working electrode, changes in the resulting voltammogram are observed upon addition of complex **1** to the electrolyte solution (Fig. 5.6). First, the potential is cycled between 1.3 and 2.0 V at 10 mV/s for five cycles with a gold working electrode in a Na_2SO_4 electrolyte solution without any metal complex present. The first scan of the resulting voltammogram shows oxidative current, associated with the formation of gold oxide, which is absent in subsequent scans (Fig. 5.6a). To demonstrate the effects of the presence of complex **1** in solution, the complex was then added to the solution, followed by another CV experiment between 1.3 and 2.0 V while keeping the resting potential at 1.3 V in between both experiments to avoid the reduction of gold oxide. The resulting voltammogram after the addition of complex **1** shows again additional oxidative current during the first scan which is absent in subsequent scans (Fig. 5.6b), despite the fact that the electrode surface had already been fully oxidized to gold oxide during the previous CV experiment shown in figure 5.6a.

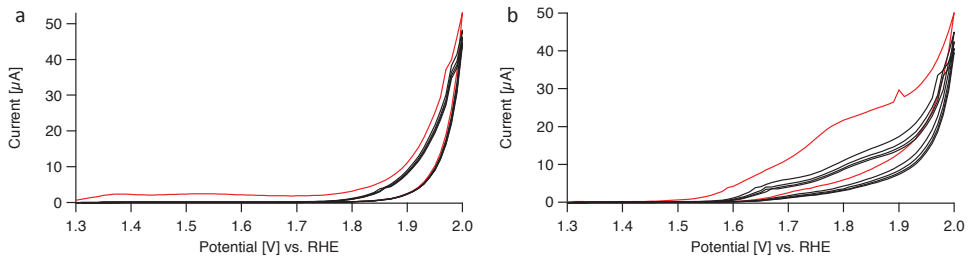

Figure 5.6: (a) Results of a CV measurement with a gold working electrode in a 0.125 M Na_2SO_4 electrolyte solution, recorded between 1.3 and 2.0 V vs. RHE at 10 mV/s, starting at 1.3 V vs. RHE. The first scan is depicted in red, subsequent scans in black. (b) Results of a CV measurement with a gold working electrode in the presence of 0.5 mM complex **1** in a 0.1 M Na_2SO_4 electrolyte solution, recorded between 1.3 and 2.0 V vs. RHE at 10 mV/s, starting at 1.3 V vs. RHE. The first scan is depicted in red, subsequent scans in black. The working electrode was pre-treated before the experiment by oxidation of the electrode surface to gold oxide by cycling five times between 1.3 and 2.0 V vs. RHE at 10 mV/s as is shown in Fig. 5.6a.

After five cycles between 1.3 and 2.0 V at 10 mV/s in the presence of complex **1**, the electrode was taken out of the electrolyte solution containing complex **1**, rinsed with Milli-Q water and placed in a fresh blank electrolyte solution of Na_2SO_4

while again applying a resting potential of 1.3 V to avoid the reduction of gold oxide. In a subsequent CV experiment, the potential was cycled between 0.0 and 2.0 V for three cycles with a starting potential of 1.3 V (Fig. 5.7a). The resulting voltammogram shows a clear difference between the first scan and the following two scans. In the first scan of the CV experiment, the first gold oxide reduction peak at 1.2 V (hereafter called peak I) is almost entirely absent and the second reduction peak at 0.7 V (hereafter called peak II) is clearly visible. In the second and third scan of the CV experiment, peak I is more prominent again while peak II is no longer visible. After recording these three scans, the electrode was left in contact with the electrolyte solution at a resting potential of 0.7 V for 30 minutes followed by another CV experiment between 1.3 and 2.0 V for 100 cycles, starting each cycle at 0.7 V. During the repeated scanning between 0.0 and 2.0 V, peak II slowly reappears over time (Fig. 5.7b). Additionally, the first shoulder of the gold oxide formation region at about 1.3 V also grows over time during repeated potential cycling.

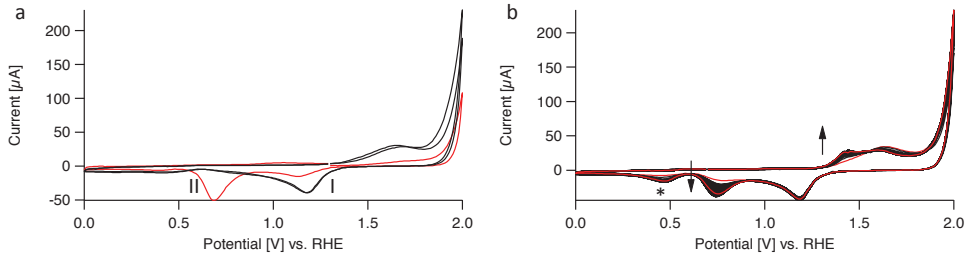

Figure 5.7: (a) Results of a CV measurement with a gold working electrode, recorded between 0.0 and 2.0 V vs. RHE in a 0.1 M Na_2SO_4 electrolyte solution, scanning at 100 mV/s, starting at 1.3 V vs. RHE. The potential was cycled three times between 0.0 and 2.0 V vs. RHE. The first scan is depicted in red, both subsequent scans in black. This CV experiment was performed after cycling the potential five times between 1.3 and 2.0 V vs. RHE at 10 mV/s in the presence of 0.5 mM complex **1** in a 0.1 M Na_2SO_4 electrolyte solution, the results of which is shown in fig. 5.6b, and subsequent rinsing of the working electrode with Milli-Q water. A resting potential of 1.3 V vs. RHE was applied before the start of the experiment to avoid premature gold oxide reduction. (b) Voltammogram of a gold working electrode after resting at 0.7 V vs. RHE for 30 min in a 0.125 M Na_2SO_4 electrolyte solution, following the experiment described under fig. 5.7a. The first and last scan are depicted in red while the intermediate scans are depicted in black. Conditions: 100 scans between 0.0 and 2.0 V vs. RHE at 100 mV/s, starting at 0.7 V vs. RHE. The arrows in the figure indicate changes in the current profile between subsequent scans. The small peak growing out at 0.5 V (indicated in the figure by an *) is due to reduction of small amounts of dioxygen formed at 2.0 V.

The fact that the reappearance of peak II only takes place during the repeated cycling and not during the 30 minute resting-period at 0.7 V means that the changes in the structure of the gold surface, which have been induced by the

presence of complex **1**, remain stable for at least 30 minutes at ambient conditions. This shows that the atoms at the surface of the gold electrode are not sufficiently mobile at room temperature and that cycling over the gold oxidation and gold oxide reduction region is crucial to achieve regeneration of the original surface structure.

To detect any influence of the pH of the electrolyte medium and to eliminate the possible influence of local pH changes at the working electrode, the same experimental procedure was repeated with a $HClO_4$ electrolyte solution instead of a Na_2SO_4 electrolyte solution for the initial and the final CV experiment in the absence of complex **1**. The CV experiment in the presence of complex **1** was performed in a 0.1 M Na_2SO_4 electrolyte solution as before. Accordingly, the gold working electrode was first oxidized in a blank 0.1 M $HClO_4$ electrolyte solution by cycling the potential five times between 1.3 and 2.0 V at 10 mV/s. The electrode was then rinsed and transferred to a different cell containing 0.5 mM complex **1** in a 0.1 M Na_2SO_4 electrolyte solution. In this solution another a CV measurement was then performed, consisting of five cycles between 1.3 and 2.0 V at 10 mV/s. After subsequent rinsing of the electrode a final CV experiment was recorded, consisting of 100 scans between 0.0 and 2.0 V at 100 mV/s in a 0.1 M $HClO_4$ electrolyte solution in the absence of complex **1**, starting each scan at 1.3 V. Throughout the entire procedure, the resting potential at the working electrode was kept at 1.3 V to avoid the reduction of gold oxide between measurements. The results of the final CV experiment in a 0.1 M $HClO_4$ electrolyte solution are summarized in figure 5.8.

The initial blank measurement of a gold background in a 0.1 M $HClO_4$ electrolyte solution before exposure complex **1** (Fig. 5.5a) showed a sharp reduction peak for gold oxide reduction at 1.1 V with a shoulder at 1.0 V. In contrast, in the first scan of the CV experiment depicted in figure 5.8, the first gold oxide reduction peak at 1.1 V is absent while the second peak at 1.0 V is strongly pronounced. In subsequent scans, the first peak is clearly visible again while the second peak is absent at first and slowly grows back over several scans. Additionally, the first shoulder of the gold oxidation current at 1.3 V also grows over time.

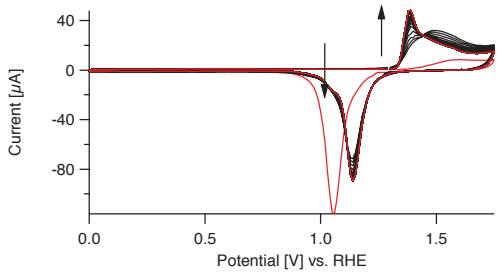

Figure 5.8: Results of a CV measurement with a gold working electrode in a 0.1 M $HClO_4$ electrolyte solution. Conditions: 100 cycles between 0.0 and 1.75 V vs. RHE in a fresh 0.1 M $HClO_4$ electrolyte solution at 100 mV/s, starting at 1.3 V vs. RHE. The electrode was pre-treated by first oxidizing the electrode surface by cycling between 1.3 and 2.0 V vs. RHE for five cycles at 10 mV/s in a 0.1 M $HClO_4$ electrolyte solution, followed by another CV measurement between 1.3 and 2.0 V vs. RHE for five cycles at 10 mV/s in a 0.1 M Na_2SO_4 electrolyte solution in the presence of complex **1** and subsequent rinsing with Mili-Q water. The resting potential at the working electrode was kept at 1.3 V vs. RHE throughout the procedure. The arrows in the figure indicate changes in the current profile between subsequent scans.

One possible explanation for these observed changes in the background voltammogram of the gold working electrode, which are apparently triggered by cyclic voltammetry between 1.3 and 2.0 V in the presence of complex **1**, could be the formation of surface deposits from complex **1** at high potentials. Those deposits could then be expelled from the surface upon repeated cycling over the gold oxide formation and gold oxide reduction potential region, which would lead to the recovery of the original background voltammogram. However, the EQCM experiments which are described in chapter 3 already rule out the formation of significant surface deposits from complex **1** in 0.1 M Na_2SO_4 electrolyte solution (see Fig 3.8, chapter 3)

A different explanation could be that restructuring of the electrode surface takes place, induced by the presence of complex **1** in solution. This explanation is also in line with results discussed in chapter 4 which already point toward restructuring processes which take place at the electrode surface in the presence of Fe(bpmcn) complexes.

The same experimental procedure that was carried out for complex **1** was repeated for complex **2** to establish whether the observed changes in the voltammogram of the gold background are exclusive for complex **1** or whether other metal complexes exhibit similar effects. Analogous to the experiment with complex **1**, the surface of the working electrode was first oxidized to gold oxide by cycling the potential between 1.3 and 2.0 V in a Na_2SO_4 electrolyte solution in the absence of any metal complex (Fig. 5.9a). To prevent gold oxide reduction, the

resting potential was kept at 1.3 V. Subsequently, complex **2** was added to the solution and another CV experiment between 1.3 and 2.0 V was performed for five cycles at 10 mV/s (Fig. 5.9b). Similar to the results obtained for complex **1**, the experiment with complex **2** also shows additional oxidative current the first scan of the voltammogram recorded after the addition of complex **2**, despite previous complete oxidation of the electrode surface to gold oxide. Also just like in the previous experiment with complex **1**, the additional oxidative current is only present in the first scan of the CV experiment after addition of complex **2** and not in subsequent scans. However, the effect of generating additional oxidative current during the first scan after addition of the complex to the electrolyte solution is less pronounced in the case of complex **2** compared to complex **1** (compare Fig. 5.9b and 5.6b).

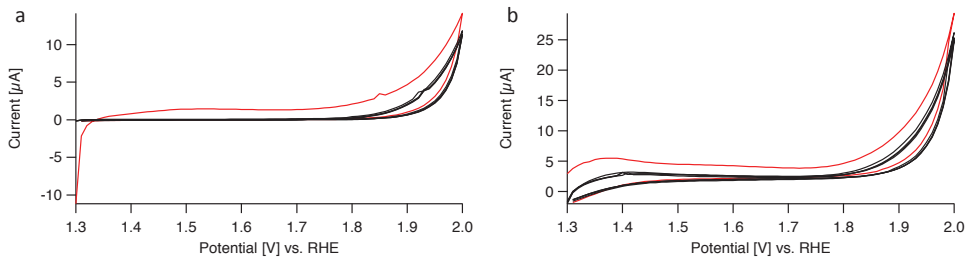

Figure 5.9: (a) Results of a CV measurement with a gold working electrode in a 0.1 M Na_2SO_4 electrolyte solution, recorded between 1.3 and 2.0 V vs. RHE at 10 mV/s, starting at 1.3 V vs. RHE. The first scan is depicted in red, subsequent scans in black. (b) Results of a CV measurement with a gold working electrode in the presence of 0.5 mM complex **2** in a 0.1 M Na_2SO_4 electrolyte solution, recorded between 1.3 and 2.0 V vs. RHE at 10 mV/s, starting at 1.3 V vs. RHE. The first scan is depicted in red, subsequent scans in black. The working electrode was pre-treated before the experiment by oxidation of the electrode surface to gold oxide by cycling five times between 1.3 and 2.0 V vs. RHE at 10 mV/s as is shown in Fig. 5.9a.

For the final step of the experiment, the electrode was taken out of the solution containing complex **2**, rinsed with Milli-Q water and placed in a cell with a fresh electrolyte solution of Na_2SO_4 without complex **2** while keeping the resting potential at 1.3 V. A CV experiment between 0.0 and 2.0 V was then recorded for 50 cycles at 100 mV/s, starting each scan at 1.3 V (Fig. 5.10).

The resulting voltammogram shows the same changes to the current profile of the gold background, compared to the initial baseline measurement before exposure to complex **2**, that were previously seen in the experiment with complex **1**. In the first scan, gold oxide reduction peak I is less pronounced compared to the initial measurement before exposure to complex **2** while reduction peak II is clearly present (Fig. 5.10a).

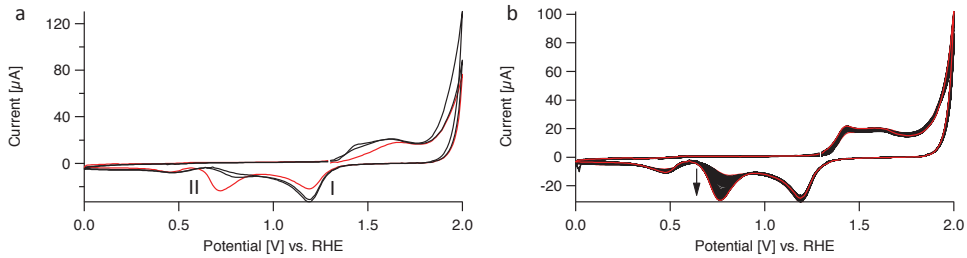

Figure 5.10: Results of a CV measurement with a gold working electrode after cycling five times between 1.3 and 2.0 V vs. RHE at 10 mV/s in the presence of 0.5 mM complex **2** in a 0.1 M Na_2SO_4 electrolyte solution (Fig. 5.9b) and subsequent rinsing of the working electrode. Shown are scans 1-3 (a) and scans 4-50 (b) of the CV experiment recorded between 0.0 and 2.0 V vs. RHE in a 0.1 M Na_2SO_4 electrolyte solution, scanning at 100 mV/s, starting at 1.3 V vs. RHE. Depicted in red are the 1st scan (a) as well as the 4th and 50th scan (b). All remaining scans are depicted in black. The arrows in the figure indicate changes in the current profile between subsequent scans.

During the second and third scan, peak I is more pronounced compared to the first scan and peak II is largely absent. In the subsequent scans peak II can be seen to grow back over time (Fig. 5.10b). However, these observed changes to the voltammogram of the gold background induced by complex **2** in solution appear to be less pronounced compared to the case of complex **1**. Gold oxide reduction peak I is still more pronounced in the first scan of the background voltammogram after exposure to complex **2** compared to the case of complex **1** (compare Fig. 5.7a and Fig. 5.10a). Additionally, gold oxide reduction peak II grows back faster over time for the case of complex **2** compared to complex **1** (compare Fig. 5.7b and Fig. 5.10b)

5.3 Conclusions

OLEMS experiments with a PG working electrode show that, contrary to previous reports, no water oxidation takes place at PG working electrodes in the absence of an additional catalyst even at potentials as high as 2.2 V vs. RHE. Instead, only CO_2 formation from the electrode material can be seen with OLEMS, starting at about 1.9 V.

In the presence of metal complexes in solution, the onset of CO_2 formation shifts to more cathodic potentials. This shift of the onset of CO_2 formation shows that high-valent metal oxo-species in solution can facilitate CO_2 formation from carbon electrodes. Depending on where the onset of CO_2 formation lies in comparison to the onset of oxygen evolution, this must be taken into consideration when analyzing the kinetics of electrocatalysts through foot-of-the-wave analysis. Furthermore, the formation of CO_2 from carbon-based electrodes is a clear

drawback compared to other electrode materials for potential sustainable fuel production applications which has to be weighed against potential benefits (cf. chapter 3).

When working with gold working electrodes, the presence of metal complexes in solution seems to induce changes in the structure of the electrode surface. These changes manifest themselves in differences in the current profile of the gold oxide formation and gold oxide reduction processes in background voltammograms of a gold working electrode, measured before and after cycling the potential between 1.3 and 2.0 V in the presence of metal complexes in the electrolyte solution. The comparison of the results obtained with complex **1** (Fig. 5.6-5.7) and complex **2** (Fig. 5.9-5.10) indicates that complex **1** interacts more strongly with the surface of the gold electrode, resulting in more pronounced changes in the background voltammogram being visible in CV experiments.

The exact nature of these changes and the mechanism through which they are induced is not yet clear. To elucidate the processes at the surface of gold working electrodes based on the recorded voltammograms, additional information is needed about the precise processes which give rise to each individual peak on an atomic level. Structural changes at the electrode surface could potentially be visualized by *in situ* spectroscopy or microscopy techniques in combination with electrochemistry.

The results presented in this chapter are in line with the results for the Fe(bpmcn) complexes discussed chapter 4, which also showed evidence for considerable interactions between the complexes and the gold electrode. On one hand, a different oxygen evolution behaviour was observed during the first scan of an OLEMS experiment compared to subsequent scans. On the other hand, the peak current at 2.0 V was found to increase between subsequent scans in CV experiments between 0.0 and 2.0 V.

In order for restructuring of the electrode surface to be induced by dissolved complexes, there must be considerable electronic interaction between the electrode surface and the complex in solution. This means that the interactions between complex and electrode go beyond simple outer sphere electron transfer mechanisms. Despite the potentially important implications for the field, at present, the interactions between metal complexes in solution and the surface of the working electrode have received little to no attention in literature on homogeneous water oxidation catalysis.

In summary, following the results discussed in chapters 3 and 4, the findings presented in this chapter further solidify the concerns that were already expressed throughout this thesis regarding the benchmarking of catalytic systems under electrochemical conditions. The results obtained for both PG and gold working electrodes show that interactions between the complexes in solution and the electrode surface significantly complicate the observed electrochemistry.
The formation of CO_2 from carbon-based electrodes is important for both benchmarking efforts and potential applications in sustainable fuel production. The interactions between dissolved metal complexes and gold working electrodes on the other hand appear to influence the structure of the electrode surface which in turn may affect for example electron transfer rates between the electrode and the catalyst. Therefore the potential influence of any interactions between dissolved complexes and the electrode surface could potentially be of critical importance and needs to be considered carefully when assessing the performance of a homogeneous electrocatalyst.

5.4 Experimental

5.4.1 General

The synthesis and characterization of complex **1** are described in chapter 3 of this thesis.
[Ru(tpy)(bpy)(H_2O)]($OTf)_2$ (**2**) was synthesized from [RuCl(tpy)(bpy)]Cl according to a modified literature procedure (see below for details).[24]
[$RuCl_3$(tpy)] and [RuCl(tpy)(bpy)]Cl were synthesized according to literature procedures.[24]

5.4.2 Electrochemical experiments

All electrochemical measurements were performed in custom made single-compartment glass cells, recorded on Ivium potentiostats, operated by IviumSoft software, using a three electrode setup with the working electrode in hanging meniscus configuration. The working electrodes used in the experiments were a pyrolytic graphite (PG) disc and a gold disc electrode. The respective (geometric) surface areas are 0.2 cm² (PG) and 0.13 cm² (gold). A large surface area gold plate was used as a counter electrode in all experiments. The reference electrode was a reversible hydrogen electrode (RHE) made up of a platinum mesh in H_2-saturated

electrolyte at the same pH as the electrolyte solution inside the cell. The cell and the reference electrode were connected via a Luggin capillary.
The PG electrode was prepared before each experiment by polishing the electrode surface with sandpaper. The polishing of the PG electrode was followed by removal of excess debris by sonicating the electrode in Milli-Q water for at least five minutes.
The gold electrode was prepared before each experiment by oxidizing the surface at 10 V for 30 s in a 10% H_2SO_4 solution, followed by stripping of the gold oxide layer in a 6 M HCl solution and subsequent electro-polishing of the electrode by scanning for 200 cycles between 0.0 and 1.75 V vs. RHE at 1000 mV/s in a 0.1 M $HClO_4$ electrolyte solution.
All glassware used in electrochemical measurements was routinely cleaned of any organic contamination by soaking in potassium permanganate solution over night. Prior to each experiment, the glassware was cleaned by threefold rinsing and boiling in Milli-Q water. All electrolyte solutions were prepared from p.a. grade chemicals (Merck Suprapur®) and Milli-Q water (resistivity ≥ 18.2 MΩ). Prior to measurements, the electrolyte solution was purged of air by bubbling with argon (Linde, Ar 6.0) for at least 20 minutes. During the measurements, the cell was constantly kept under argon flow to prevent air from entering.
For the OLEMS measurements, the gasses formed at the working electrode were collected via a hydrophobic tip (KEL-F with a porous Teflon plug) in close proximity to the surface of the working electrode and analyzed in a QMS 200 mass spectrometer. A detailed description of the OLEMS setup is available elsewhere.[25] For the mass spectrometry data recorded during cyclic voltammetry experiments, background correction was done by assuming an exponential decay fit (concerns figure 5.3).

*5.4.3 Synthesis of [Ru(tpy)(bpy)(H_2O)]($OTf)_2$ (**2**)*

[RuCl(tpy)(bpy)]Cl (200 mg, 0.36 mmol) was dissolved in 25 mL of a mixture of 75% acetone and 25% water. AgOTf (183 mg, 0.72 mmol) was added and the mixture was refluxed for 1 h. The mixture was allowed to cool down to room temperature before being filtered over celite to remove all of the formed AgCl. After evaporation of the solvent in vacuum, the obtained crude material was recrystallized from a minimal amount of acetone and water mixture (75:25) in the fridge. Yield: 122 mg (0.15 mmol, 42%)

ESI-MS (H_2O) calcd. for $C_{25}H_{19}N_5Ru$ $[M]^{2+}$ 245.5; Found: $[M]^{2+}$ 245.3, $[M+H_2O]^{2+}$ 254.2

Elemental analysis calcd. (%) for $C_{27}H_{21}F_6N_5O_7RuS_2$ (806.67 g/mol): C 40.20, H 2.62, N 8.68 Found: C 40.43, H 2.79, N 8.73.

^{1}H NMR (400 MHz, D_2O) δ [ppm] = 9.50 (d, *J* = 5.7 Hz, 1H), 8.64 (d, *J* = 8.2 Hz, 1H), 8.55 (d, *J* = 8.1 Hz, 2H), 8.42 (d, *J* = 8.1 Hz, 2H), 8.29 (m, 2H), 8.18 (t, *J* = 8.1 Hz, 1H), 7.99 (ddd, *J* = 7.3, 5.6, 1.3 Hz, 1H), 7.93 (ddd, *J* = 7.9, 1.5 Hz, 2H), 7.77 (d, *J* = 5.7 Hz, 2H), 7.64 (ddd, *J* = 7.9, 1.5 Hz, 1H), 7.34-7.24 (m, 3H), 6.89 (ddd, *J* = 7.4, 5.8, 1.3 Hz, 1H).

5.4.4 Sample preparation

Due to slow dissolution of complex **1** in 0.1 M Na_2SO_4 electrolyte solution, the complex was initially dissolved in a small amount of Milli-Q water (typically 1-2 mL) and subsequently added to the electrochemical cell containing the electrolyte solution. The concentration of electrolyte in the cell was adjusted to account for the resulting dilution. To achieve faster dissolution of complex **1** in water the crystals were powderized before dissolving them in water.

For electrochemical experiments with complex **1**, the complex was dissolved in air-saturated Milli-Q water and subsequently added to the electrochemical cell after complete dissolution. The electrolyte was then purged again of air by bubbling with argon for several minutes.

For electrochemical experiments with complex **2**, the complex was sonicated in a few mL of the electrolyte solution to achieve complete dissolution and subsequently added to the electrochemical cell. The electrolyte was then purged again of air by bubbling with argon for several minutes.

All experiments with complex **1** and **2** were performed at a concentration of 0.5 mM unless otherwise specified.

5.5 References

[1] J. D. Benck; B. A. Pinaud; Y. Gorlin; T. F. Jaramillo, *PLoS One* **2014**, *9*, e107942.

[2] A. M. Ullman; Y. Liu; M. Huynh; D. K. Bediako; H. Wang; B. L. Anderson; D. C. Powers; J. J. Breen; H. D. Abruna; D. G. Nocera, *J. Am. Chem. Soc.* **2014**, *136*, 17681-17688.

[3] S. Fukuzumi; D. Hong, *Eur. J. Inorg. Chem.* **2014**, *2014*, 645-659.

[4] B. Limburg; E. Bouwman; S. Bonnet, *Coord. Chem. Rev.* **2012**, *256*, 1451-1467.

[5] O. Diaz-Morales; F. Calle-Vallejo; C. de Munck; M. T. M. Koper, *Chem. Sci.* **2013**, *4*, 2334.

[6] K. G. Kottrup, *This Thesis, Chapter 3*.
[7] Y. Yi; G. Weinberg; M. Prenzel; M. Greiner; S. Heumann; S. Becker; R. Schlögl, *Catal. Today* **2017**, *295*, 32-40.
[8] R. Matheu; M. Z. Ertem; J. Benet-Buchholz; E. Coronado; V. S. Batista; X. Sala; A. Llobet, *J. Am. Chem. Soc.* **2015**, *137*, 10786-10795.
[9] C. Costentin; S. Drouet; M. Robert; J. M. Saveant, *J. Am. Chem. Soc.* **2012**, *134*, 11235-11242.
[10] H. Angerstein-Kozlowska; B. E. Conway; A. Hamelin; L. Stoicoviciu, *Electrochim. Acta* **1986**, *31*, 1051-1061.
[11] H. Angerstein-Kozlowska; B. E. Conway; A. Hamelin; L. Stoicoviciu, *J. Electroanal. Chem. Interfacial Electrochem.* **1987**, *228*, 429-453.
[12] Z. Borkowska; A. Tymosiak-Zielinska; G. Shul, *Electrochim. Acta* **2004**, *49*, 1209-1220.
[13] A. Hamelin, *J. Electroanal. Chem.* **1996**, *407*, 1-11.
[14] A. Hamelin; A. M. Martins, *J. Electroanal. Chem.* **1996**, *407*, 13-21.
[15] B. B. Blizanac; C. A. Lucas; M. E. Gallagher; M. Arenz; P. N. Ross; N. M. Marković, *J. Phys. Chem. B* **2004**, *108*, 625-634.
[16] L. D. Burke; P. F. Nugent, *Gold Bull.* **1997**, *30*, 43-53.
[17] L. D. Burke; P. F. Nugent, *Gold Bull.* **1998**, *31*, 39-50.
[18] A. Hamelin; M. J. Sottomayor; F. Silva; S.-C. Chang; M. J. Weaver, *J. Electroanal. Chem. Interfacial Electrochem.* **1990**, *295*, 291-300.
[19] B. Lertanantawong; A. P. O'Mullane; W. Surareungchai; M. Somasundrum; L. Declan Burke; A. M. Bond, *Langmuir* **2008**, *24*, 2856-2868.
[20] M. J. Nicol, *Gold Bull.* **1980**, *13*, 46-55.
[21] M. J. Nicol, *Gold Bull.* **2013**, *13*, 105-111.
[22] A. Hamelin; L. Stoicoviciu, *J. Electroanal. Chem. Interfacial Electrochem.* **1987**, *234*, 93-105.
[23] A. Hamelin; L. Stoicoviciu, *J. Electroanal. Chem. Interfacial Electrochem.* **1987**, *236*, 267-281.
[24] K. J. Takeuchi; M. S. Thompson; D. W. Pipes; T. J. Meyer, *Inorg. Chem.* **1984**, *23*, 1845-1851.
[25] A. H. Wonders; T. H. M. Housmans; V. Rosca; M. T. M. Koper, *J. Appl. Electrochem.* **2006**, *36*, 1215-1221.